Australasian Physical & Engineering Sciences in Medicine (2019) 42:573–584
https://doi.org/10.1007/s13246-019-00759-0

SCIENTIFIC PAPER

Artificially enriching the training dataset of statistical shape models via constrained cage-based deformation

Samaneh Alimohamadi Gilakjan[1,2] · Javad Hasani Bidgoli[3] · Reza Aghaizadeh Zorofi[3] · Alireza Ahmadian[1,2]

Received: 17 June 2018 / Accepted: 27 April 2019 / Published online: 13 May 2019

Abstract

The construction of a powerful statistical shape model (SSM) requires a rich training dataset that includes the large variety of complex anatomical topologies. The lack of real data causes most SSMs unable to generalize possible unseen instances. Artificial enrichment of training data is one of the methods proposed to address this issue. In this paper, we introduce a novel technique called constrained cage-based deformation (CCBD), which has the ability to produce unlimited artificial data that promises to enrich variability within the training dataset. The proposed method is a two-step algorithm: in the first step, it moves a few handles together, and in the second step transfers the displacements of these handles to the base mesh vertices to generate a real new instance. The evaluation of statistical characteristics of the CCBD confirms that our proposed technique outperforms notable data-generating methods quantitatively, in terms of the generalization ability, and with respect to specificity.

Keywords Statistical shape model · Training dataset · Artificial data · Constrained cage-based deformation · Generalization ability · Specificity

Introduction

Statistical shape models (SSM) are the solution for a variety of biomedical applications such as image analysis [1, 2] registration [3, 4] and shape deformation [5]. Further, segmentation is one of the other interesting applications of SSMs in parts of the body such as the spine [6], femur and pelvis [7], liver [8, 9], prostate [10], hip [11], and heart [12–14]. SSMs are constructed by learning the variations in the training dataset. Consequently, their performance is highly influenced by the richness of the training data.

Generally, the over-constraining problem restricts SSMs from generalizing the possible new, real, and unseen instances. Various researchers, who have used SSMs with different applications, have noted this issue and the corresponding negative impact on their performances. Mitchell et al. constructed an Active Appearance model (AAM) using 55 subjects and realized that their AAM fails to consider local appearance variations owing to the limited number of the training set [15]. Davatzikos et al. found that although using 50 samples is sufficient for constructing an Active Shape model for simple structures, this data size is insufficient for complex ones [16]. Global characteristics could be captured by lower bands, and higher bands are responsible for the local shape variations; the wavelet transform was utilized to benefit from this feature. Chung et al. announced that by using statistical methods, the results of the segmentation of the lower limb bones in MRI images is improved when the number of the training datasets is increased [17]. Ordas et al. concluded that SSMs that take advantage of the

✉ Alireza Ahmadian
ahmadian@sina.tums.ac.ir

Samaneh Alimohamadi Gilakjan
s-alimohamadi@razi.tums.ac.ir

Javad Hasani Bidgoli
jbidgoli@razi.tums.ac.ir

Reza Aghaizadeh Zorofi
zoroofi@ut.ac.ir

1 Department of Biomedical Systems & Medical Physics, Tehran University of Medical Sciences, Tehran, Iran

2 Research Center for Biomedical Technologies and Robotics, Imam Khomeini Hospital Complex, Keshavarz Blvd, Tehran, Iran

3 Control & Intelligent Processing, Center of Excellence, School of Electrical and Computer Engineering, College of Engineering, University of Tehran, Tehran, Iran

large variation of shape information are able to represent a larger number of flexible instances [18].

Different methods of solution have been proposed to improve SSMs. One such method is based on the idea that each complex structure comprises several simpler components that can be modeled separately with fewer training data. De Bruijne et al. used a shape model to consider the general structures, and an intensity model to capture the local elegant variations in order to segment aortic aneurysms accurately [19]. Hu et al. proposed a new method based on non-uniform rational B-spline to generate large datasets from the limited number of cone-beam computed tomography images to derive real variables in SSM construction that can be used in adaptive radiotherapy purposes [20]. A recent research [21, 22] merging pre-existing SSM properties without the need for the original data has been published. The authors claim that their model is capable of representing global and local features of complex objects. Using a patch-based technique, Ehrhardt et al. overcame the restricted access to the training data in SSM construction. Their proposed approach uses a low-rank matrix completion method and makes it possible to learn a large number of details from the small amount of training data available [23].

Besides the researchers who tried to use existing real data, other research groups attempted to enrich the statistical model's training dataset in a different manner: by producing artificial real appearance data. For example, Cootes and Taylor expanded the vibration modes via the finite element method and generated new modified instances even in the absence of the adequate number of datasets [24]. Lötjönen et al. proposed several methods to artificially enlarge the data and evaluated their methods by comparing the segmentation results of the 3D cardiac MRI data [13]. They claim that enlargement based on the non-rigid movement method delivered the best results. Koikkalainen et al. developed a method to enlarge the data artificially and made a model of a four-chamber heart [25]. They evaluated their method through SSM-based segmentation and concluded that the increased number of vibration modes could improve the segmentation result.

Cage-based deformation (CBD) is a method for artificial data generating in computer graphics applications [26, 27]. This method was first used to impart smooth motion to animated characters. For this purpose, some handles that make a cage were located in different positions of the object by the user. Figure 1 shows an example of such a cage comprising a number of handles, shown as yellow dots, inside and outside the body of an animation character. A weighted linear combination of these handles' affine transformations then results in the deformation of the object. CBD has two main capabilities: realistic convenient deformation that can preserve high-frequency details [26, 27], and using arbitrary

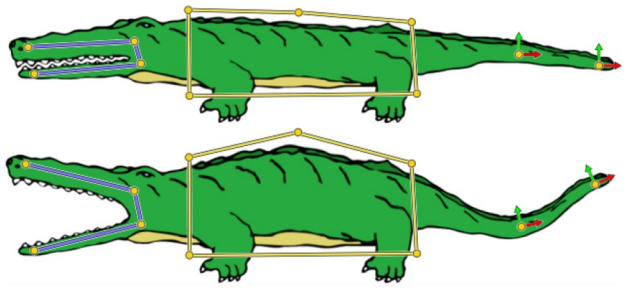

Fig. 1 Deformation of an animated character by the linear combination of the affine transformations of the handles inside and outside the object [26]

irregular control points based on the demanded deformation by considering a large and small number of control points in high detailed and smooth regions, respectively. Preserving the details of the topology and smoothness during deformation is the most important issue considered by researchers in various computer graphics applications, such as the positive mean value [28] and harmonic coordinates [29].

To the best of our knowledge, this is the first time that the concept of animation object morphing has been improved and is intended to enlarge the training set of SSMs for use in biomedical applications. Additional constraints have also been applied to the handles in the proposed CCBD method to make a global deformation in each handle movement and to prevent unreal data generating. The proposed approach can be repeated to any number desired by the user. The statistical characteristics of the enlarged SSM of the CCBD, have been compared with other methods for enlargement of the training dataset, such as non-rigid movement (NRM) [13, 25], principal component analysis–finite element model (PCA–FEM) [24], blind covariance matrix editing [30, 31], and standard PCA. The remainder of this paper is organized as follows: section "Materials and methods" provides information regarding the dataset and describes the proposed method, cage generation, CCBD, and the enhanced SSM. Section "Results" shows the evaluation results of generalization ability, specificity and the repeatability. The final sections of the paper contain the "Discussion" and "Conclusion".

Materials and methods

Dataset

In this study, 3D CT images of 50 livers [32] used acquired by the Siemen scanner with in-slice resolution ranges from 0.97 to 1.36 mm and the slice thickness between 3.37 and 5 mm. In addition, 3D CT images of 42 femurs used with in-slice resolution ranging from 0.46 to 0.88 mm and slice

thickness of 1.00 to 2.00 mm. The femur dataset acquired by Toshiba and GE CT scanners in Imam Khomeini Hospital, Tehran, Iran.

Method

Strengthening the statistical model via artificial data generation commences with providing a small amount of real data. Here the available data are 3D CT images of the liver and femur. 3D models of these images are constructed using their segmentation and meshing. The vertices and faces of the 3D model generated by applying a technique proposed by Fang et al. [33]. This powerful method creates a surface or volumetric mesh from binary or gray-scale medical images and can mesh challenging structures such as volumes of multiple regions and opened surfaces, robustly. These 3D meshes are considered to be the base models, and their deformation using handles creates artificial data. Finally, the enlarged SSM is constructed using real and artificial data, and its statistics are compared with those of the model made only from the primary real data. Once the 3D base models are made, cage generation, CBD and lastly, constraining the CBD, as described below, are carried out in order to build an optimized SSM.

Cage generation

The cage is made by placing handles inside or outside of the 3D model of the real data. However, it has been heuristically observed that a smoother warped model can be created using an internal cage. Since the 3D model is deformed by its cage, they should have a similar topology. To achieve this, a decimated version of the base model creates the cage. [34]. Building the decimated version is easy and prevents from manually locating the handles around the base model.

Figure 2a depicts the 3D model of a liver with its decimated version as the cage, which is depicted as red dots on the surface. The low-resolution version of the base model is created using a mesh decimation algorithm [34]. The smart point selection of this algorithm preserves the overall shape of the mesh by retaining the points that are visually important. Next, the selected vertices move normal to the surface as indicated by the black arrow. The new positions, shown with blue dots in Fig. 2a and b, make the cage. The movement in the normal direction prevents the shape from collapsing.

CBD

To create a deformation in the base model using cage handles, we need to explain the relationship between them using computer graphics theories.

In CBD, an object is warped based on the handles' transformations. In this way, the following equation defines the new position of the object vertices after warping [35, 36]:

$$\acute{p}_i = \sum_{h=1}^{H} w_i^h \cdot T_h \cdot \begin{pmatrix} \boldsymbol{p_i} \\ 1 \end{pmatrix} \tag{1}$$

where p_i is the initial position of the base model vertex, T_h is a deformation transform for handle h (which will be explained later), w_i^h is the blending coefficient, and $\acute{p}_i$ is the transformed point.

Blending coefficients are a set of real coefficients with two main constraints: (1) they are positive, and (2) the sum of the coefficients is normalized to 1 with respect to p_i. These coefficients help to describe the coordinates of each point of the mesh based on the other points. The bounded bi-harmonic blending method [26] has been selected here to calculate the blending coefficients among the available methods, such as mean value coordinate [37], green coordinate [38], positive mean value coordinate [28] and harmonic coordinate [29], owing to making smooth and intuitive morphing [26]. These coefficients are calculated only once; therefore, fast warping is accessible owing to the linear blending computation

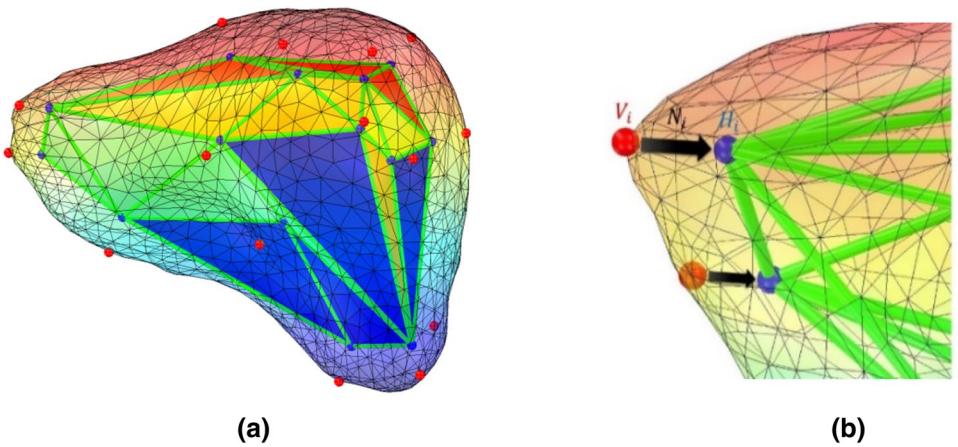

Fig. 2 3D model of the liver and its internal cage. Red and blue dots represent the vertices of the decimated (V_i) and cage (H_i) models of the liver, respectively

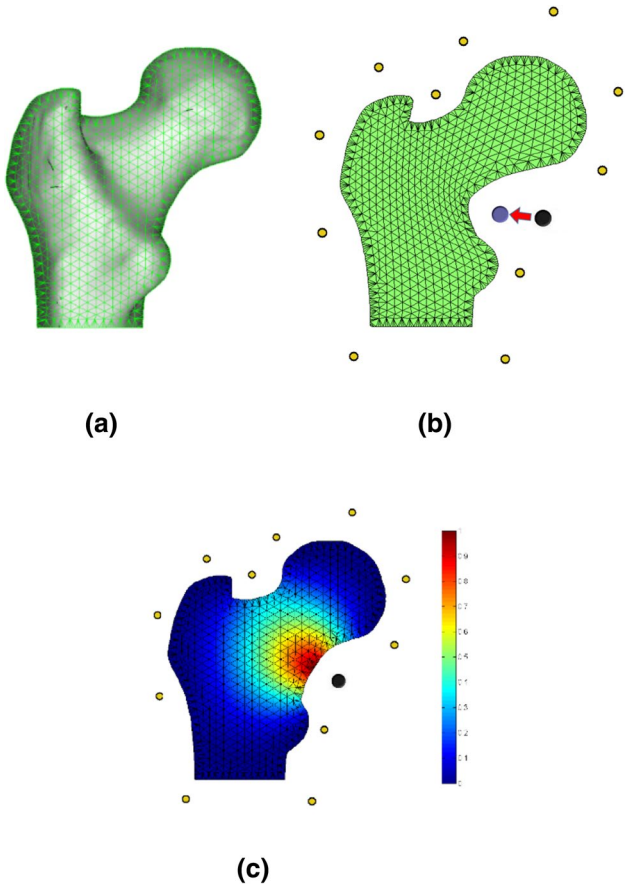

Fig. 3 Typical warping of medical data via the CBD through the displacement of a cage handle. **a** A femur-triangulated mesh. **b** Warped femur model after handle displacement (The blue handle shows the new position of the original black handle). **c** Color-coded graphical illustration of the blending coefficients of the black handle

during deformation through Eq. 1. Considering the above equation, each model vertex p_i is warped to $\acute{p}_i$; hence, the entire shape will be warped. Figure 3 depicts the typical warping of a femur model by displacing one of the cage handles.

Constrained CBD

Equation 1 describes how the handles transform back to the mesh and deform it. Transforming the handles is explained in the following equation.

Linear differential coordinates [39] is defined based on the weighted sum of the difference between the absolute coordinates of a handle and its direct neighbors.

$$\delta_i = \sum_{j \in N(i)} s_{ij}\left(v_i - v_j\right) \tag{2}$$

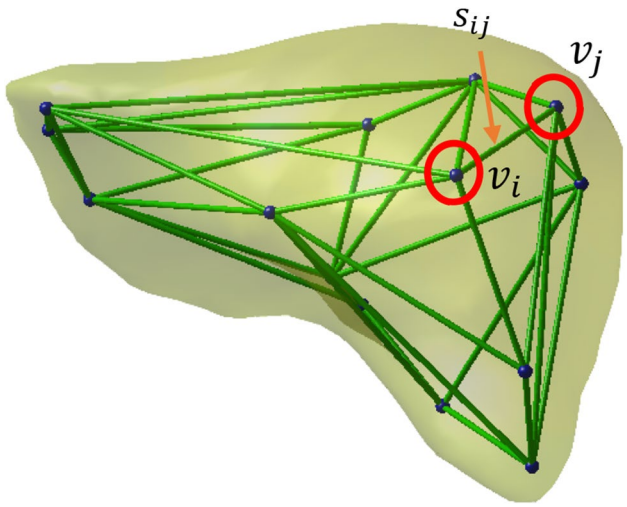

Fig. 4 Internal cage of the liver shown in Fig. 2. One sample handle and its direct neighbors with a connecting weight

v_j are the direct neighbors of the handle v_i, and s_{ij}, the stiffness parameter, is the connecting weight of the handles v_i and v_j. Some of the common stiffness parameter choices are uniform and cotangent-weights [40]. In fact, the stiffness parameter determines the locality impact of the movement of each handle on other handles. Figure 4 shows only the internal cage of the liver that was previously depicted in Fig. 2. As can be seen, s_{ij} is the connecting weight of the v_i and one of its direct neighborhood handles v_j, which are depicted as blue dots.

The Laplace–Beltrami equation describes the above concept for all cage handles as follows:

$$\delta = Lx \tag{3}$$

where δ denotes the differential coordinates [39], L is the Laplace–Beltrami matrix of the handles, and x is the absolute position of the handle. Establishing this relation between handles causes the movement of each handle to affect others; therefore, by shifting only one handle, all the handles are moved. The new location of all the handles after moving one of them is the unknown that we are looking for. This can be solved by adding the new position of the selected handle as a soft constraint to the equation. The soft constraint is a subset of linear constraints in the form of q = Cx.

In this way, the answer needs to approximately satisfy the constraint and the equation will change as follows:

$$\begin{pmatrix} \delta \\ q \end{pmatrix} = \begin{pmatrix} L \\ C \end{pmatrix} x \tag{4}$$

A solution for the above equation to find the new position of all the handles could be fined by the minimization of this equation:

$$argmin\left\{ \| Lx - \delta \|^2 + \| Cx - q \|^2 \right\} \tag{5}$$

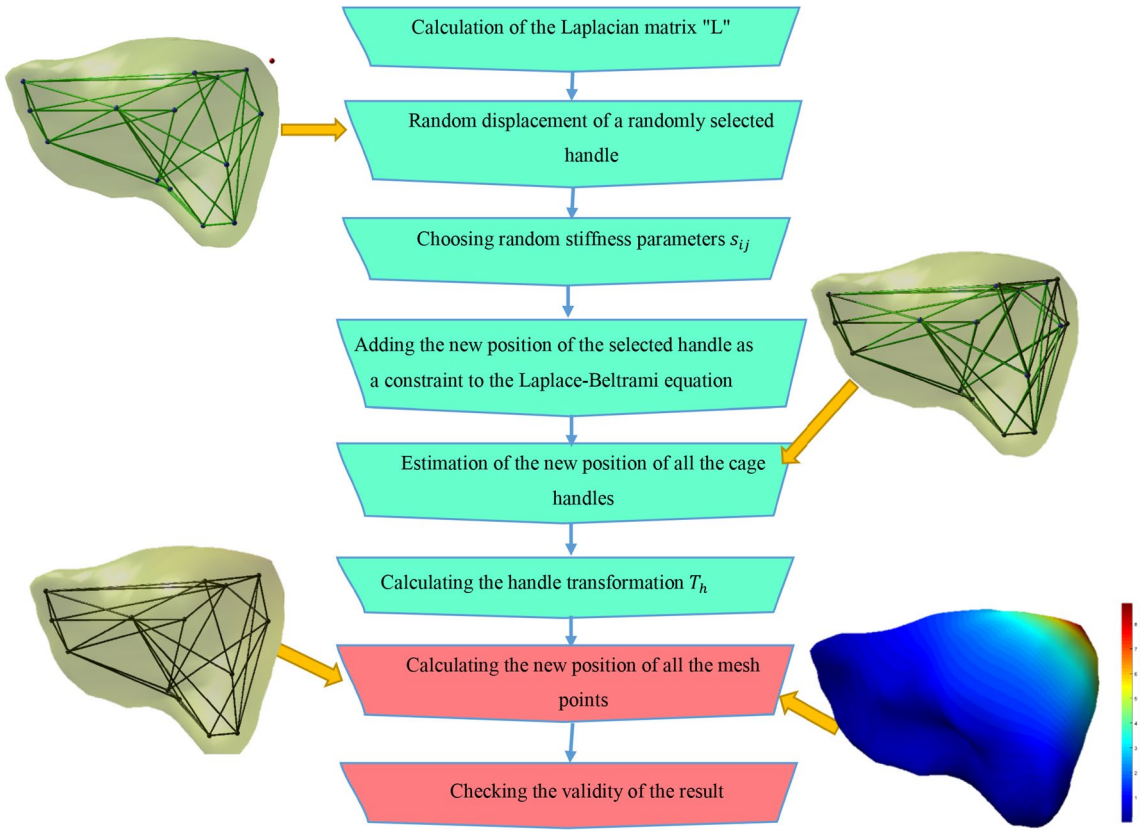

Fig. 5 Block diagram for the proposed two-step algorithm. The first and second steps are represented by green and pink blocks, respectively

In summary, the proposed algorithm can be seen in the form of a seven-step deformation algorithm as the block diagram illustrated in Fig. 5. First of all, the Laplacian matrix *"L"* of the cage handles calculates. Then one of the cage handles is randomly selected and displaced to a new position, randomly. In this step, the stiffness parameters s_{ij} are chosen randomly. Next, the new position of the selected handle adds to the Laplace–Beltrami equation as a constraint, and the new position of all the cage handles estimated. Here the transformation between the old and new positions of the selected handle, T_h can be calculated. In this point, the new position of all the points on the mesh could be calculated solving the linear equation of (1), and therefore the new deformed shape will be obtained very fast. At the final step, the validity of the result checks by an expert and the unrealistic auxiliary generated data will be excluded. So, through a 7-step algorithm (Fig. 5), the new artificial models are created and help to enrich the SSM.

Figure 6 shows artificial models of the liver and femur using the proposed CCBD method. For a better intuitive understanding of the difference between the artificial model created and the base model, the color coding has been used. As can be seen, the proposed method is able to change the shapes to create a variety of real instances. The difference between the instances created is more visible in femoral images, particularly in the femoral head, trochanter, and the epicondyle in the lower femur.

Enhanced SSM (ESSM)

As described in the previous section, using the proposed two-step algorithm with the steps mentioned, new artificial instances will be generated. The data generated are checked out in the last step to exclude those that are not looking good out of the dataset. Data exclusion criteria include the presence of sharp edges or deformation in such a way that the artificial data's overall shape is destroyed such as examples shown in Fig. 7. The ESSM will be created using the remaining data.

One of the most critical steps hereafter in constructing SSMs is to find the corresponding vertices of the training data that is done here using a non-rigid iterative closest

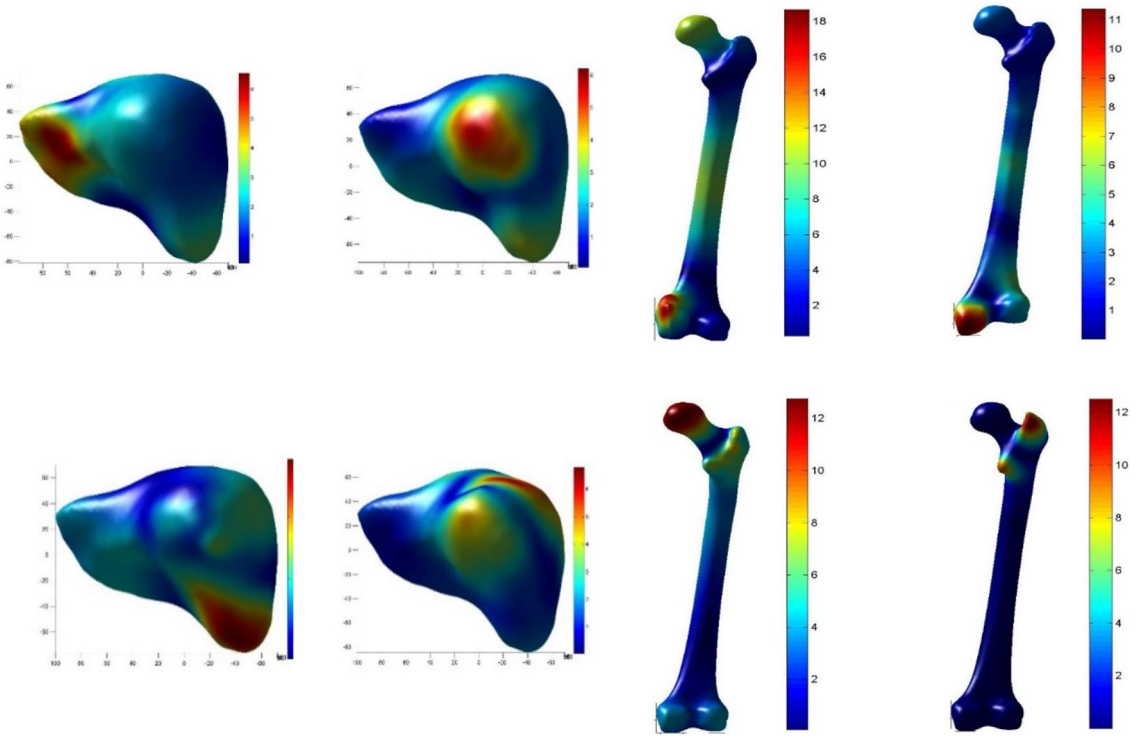

Fig. 6 Randomly generated artificial liver (left images) and femur (right images) models using the proposed CCBD method. The color coding indicates the deformation compared with the original model

point (ICP) algorithm [41]. Dimensionality reduction as the next step is accomplished using principal component analysis (PCA) [42] and finally, averaging over all the data, generates the enhanced statistical mean model.

Result

In this section, the statistical benefits of the axillary dataset have been studied. It must be emphasized that the warped models were randomly generated according to the details discussed in the previous section and no user interaction has been done in model warping. In addition to evaluating the generalization ability [43], the specificity [43] assessment has been conducted. The generalization ability expresses the model prediction error of unseen instances, and the specificity indicates the model's ability to generate instances similar to those presented in the training set.

Generalization ability

The most important SSM characteristic to be analyzed is the generalization ability, which measures an algorithm's ability to predict previously unseen instances through a leave one out approach. To quantitatively assess the performance of the proposed technique, we compared it with some notable existing methods in this field, such as NRM [13, 25], PCA–FEM [24], blind covariance matrix editing [30, 31] and standard PCA. The process of training the SSM is conducted using real data with the artificial data created by the proposed algorithm. In the dimensionality reduction step [42], only a few of the modes were used. Finally, the evaluations were performed using the following equation [43].

$$G(L) = \frac{1}{n_{test}} \sum_{i=1}^{n_{test}} \left(D\left(M_i, M_i'(L)\right) \right) \tag{6}$$

where n_{test} is the number of test data, $M_i'(L)$ is the reconstructed model of M_i using L dominant eigenvector and $D(.,.)$ indicates the distance computed between the shapes.

Figure 8 compares the generalization ability of our proposed method with other methods mentioned before for liver and femur. In this figure, 10 and 30 real data have been merged with more than 80 artificial data, and the generalization ability assessment has been conducted out with respect to the number of modes. Each of the shapes individually indicates that regardless of the actual number of real data used, the proposed method has a better generalization ability than other methods.

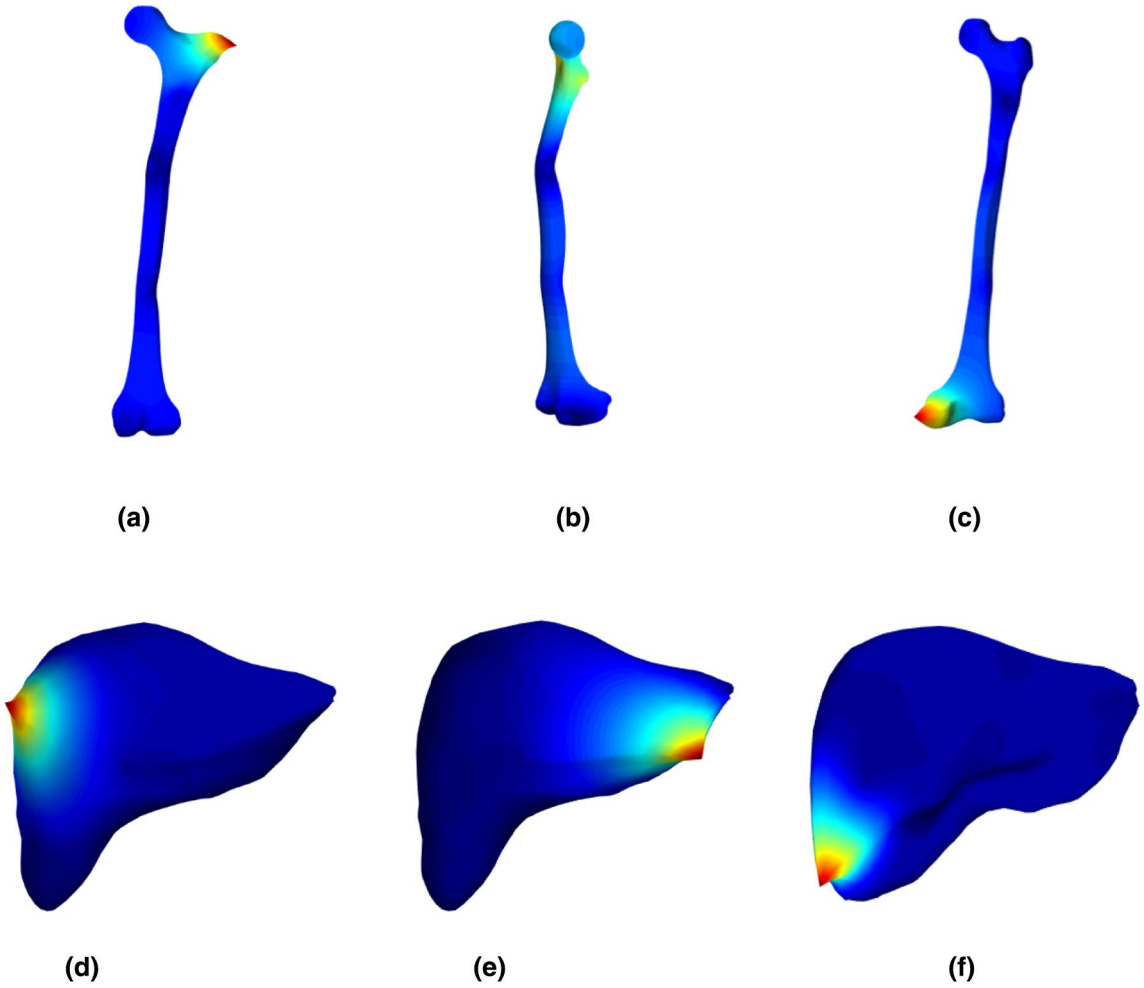

Fig. 7 Examples of sharpness and data deformity for auxiliary generated femur (**a**, **b**, **c**) and and liver (**d**, **e**, **f**)

Specificity

Another evaluation performed on the ESSM model is that of specificity, which measures the similarity of the artificial data generated with real data, according to the following equation [43].

$$S(L) = \frac{1}{n_{test}} \sum_{j=1}^{n_{test}} \min \sum_{i=1}^{N} (D(M_j, M_i'(L)) \tag{7}$$

where $M_i'(L)$ is the set of N artificial data generated. A value of $N = 10{,}000$ is used for evaluation in this paper.

The results are shown in Fig. 9 for the liver and femur. The graph indicates that the constructed CBD SSM has better specificity than other data-generating methods.

Repeatability

To support the claim that the CCBD algorithm can be repeated to any number desired by the user, a test was arranged starting with 20 real data. Then 100 artificial models were generated for each of the real data separately. All 2000 created artificial data were divided into four groups of 500, randomly and finally, 20 real data was added to all the groups and the generalization ability and robustness of the entire process evaluated. The results are shown in the following figure and table (Fig. 10; Table 1).

As can be seen, there is no significant difference between the four groups which indicates the robustness of the algorithm.

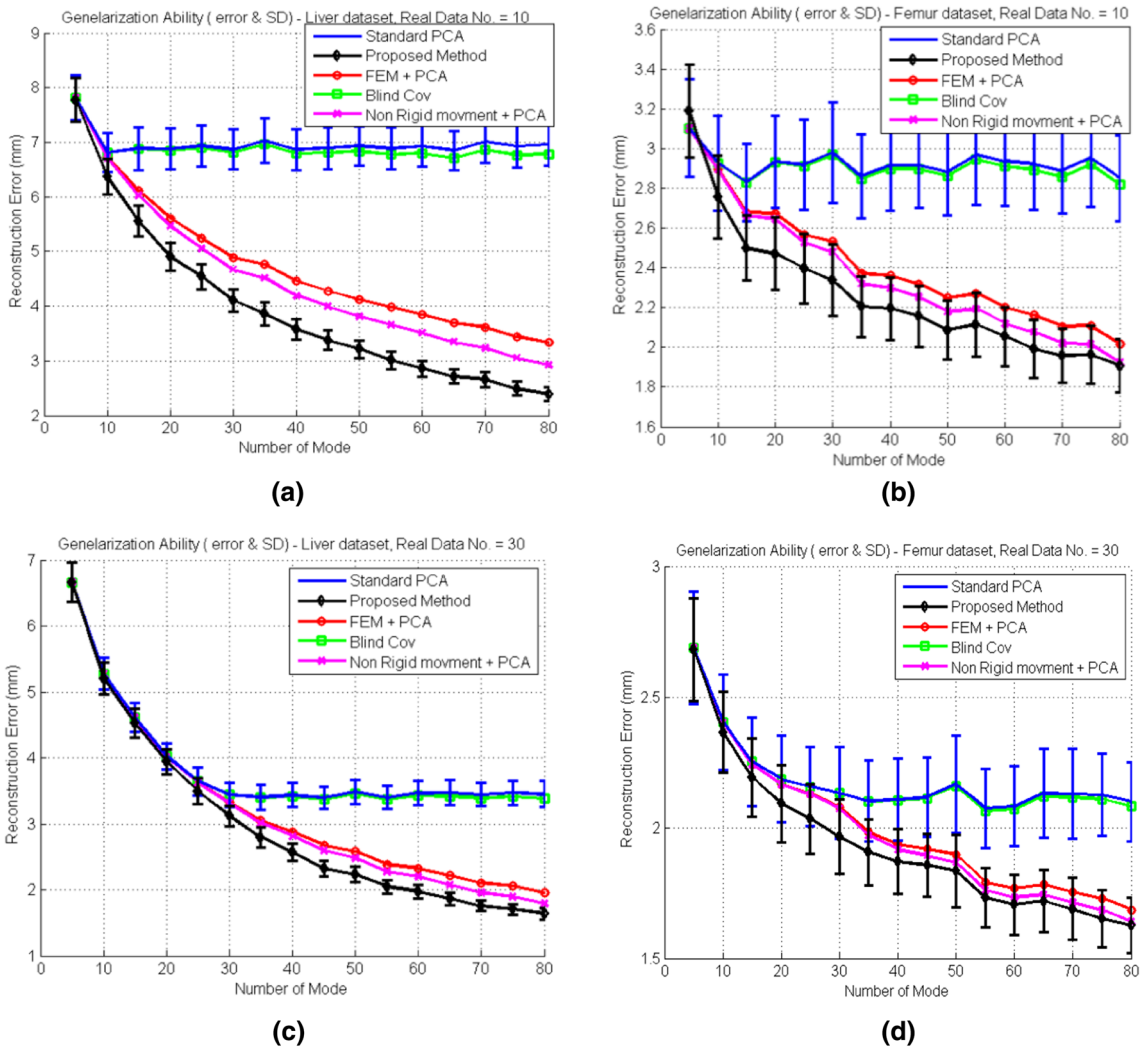

Fig. 8 Generalization ability and standard deviation of ESSM based on 10 (**a** and **b**) and 30 (**c** and **d**) real data according to the number of modes for liver (left column) and femur (right column)

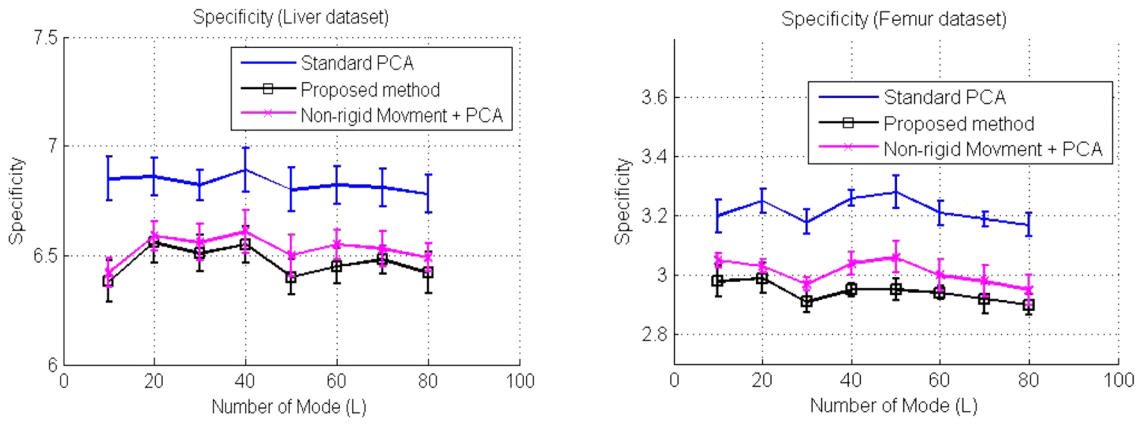

Fig. 9 Specificity comparison of standard PCA, NRM and proposed method using 15 real data with respect to the number of modes for liver (left) and femur (right) models

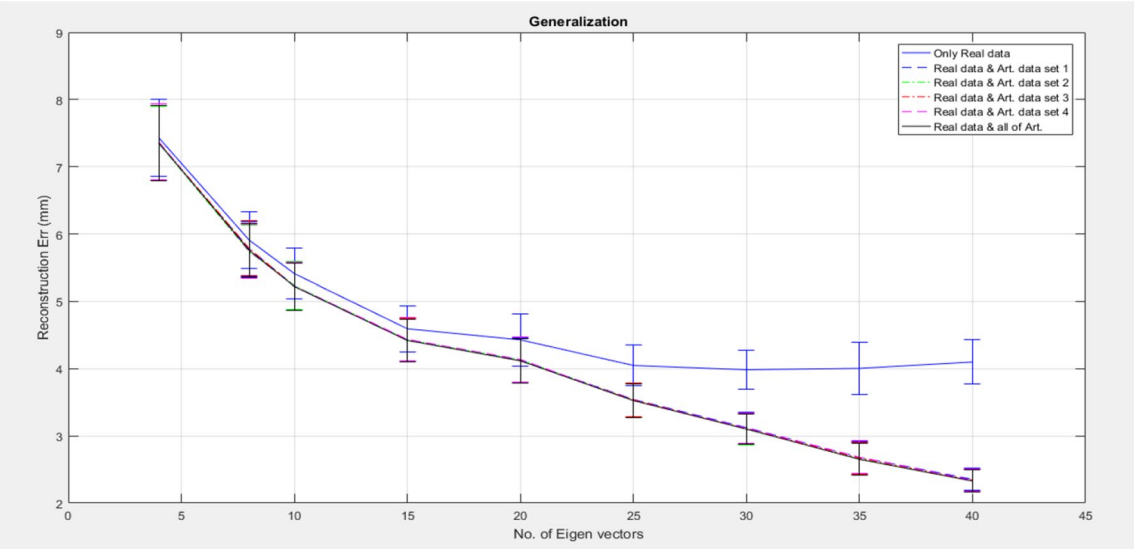

Fig. 10 The reconstruction error for real along with the artifitial data with respect to the number of modes

Table 1 Numeical generalization error with different training datasets with respect to the number of modes

Number of Modes									
	4	8	10	15	20	25	30	35	40
Only real data	7.43 ± 0.57	5.91 ± 0.43	5.41 ± 0.38	4.59 ± 0.34	4.43 ± 0.39	4.05 ± 0.30	3.98 ± 0.29	4.00 ± 0.38	4.10 ± 0.33
Real data + set 1 of artificial	7.35 ± 0.56	5.78 ± 0.41	5.23 ± 0.36	4.43 ± 0.32	4.13 ± 0.33	3.54 ± 0.25	3.12 ± 0.23	2.68 ± 0.23	2.35 ± 0.16
Real data + set 2 of artificial	7.35 ± 0.56	5.74 ± 0.40	5.24 ± 0.35	4.43 ± 0.32	4.13 ± 0.33	3.53 ± 0.25	3.10 ± 0.23	2.66 ± 0.24	2.33 ± 0.16
Real data + set 3 of artificial	7.36 ± 0.55	5.79 ± 0.41	5.22 ± 0.35	4.42 ± 0.32	4.12 ± 0.33	3.54 ± 0.25	3.11 ± 0.23	2.67 ± 0.24	2.34 ± 0.16
Real data + set 4 of artificial	7.37 ± 0.56	5.75 ± 0.40	5.23 ± 0.35	4.44 ± 0.32	4.14 ± 0.34	3.53 ± 0.25	3.11 ± 0.23	2.68 ± 0.24	2.34 ± 0.16

Generalization error (mean ± Std)

Number of real data: 20

Discussion

The introduced workflow, constrained cage-based deformation, which is a constraint version of the CBD in the biomedical field, contributes to the enrichment of the statistical model by generating artificial data. The statistical characteristics of the CCBD were evaluated quantitatively by comparing them with other well-known techniques in terms of the parameters such as generalization ability and specificity.

The liver generalization assessment demonstrates a 64% average improvement over the worst cases, standard PCA and blind covariance, for ten real data numbers and in the presence of 80 modes. The improvements compared with the PCA–FEM and non-rigid movements are 28% and 16%, respectively, in the same situation. When the real data number increases to 30, the improvement is approximately 50% for standard PCA and blind covariance and 15% and 8% for the PCA–FEM and NRM, respectively.

The generalization assessment for 10 femoral data shows a betterment of approximately 34% compared with standard PCA and blind covariance, and approximately 5% and 1% compared with the PCA–FEM and NRM, respectively. Improvement with 30 femoral data is approximately 25% relative to both standard PCA and blind covariance and approximately 6% and 3% compared with the PCA–FEM and NRM, respectively.

Regarding specificity, the outcomes represent a 6% and 8% improvement for the liver and femur, respectively.

The numbers mentioned above indicate that the method presented here makes a remarkable improvement over the

standard PCA and blind covariance while being comparable with PCA–FEM and NRM. In addition, comparing sections (a) and (b) for the liver and (c) and (d) for the femur data shows that more real data yields better results. Although this rational result is expected, when faced with the lack of real data, the proposed method can cover this issue to a large extent.

When the CCBD is compared with other methods, it can be claimed that a local deformation scheme with a global effect is proposed in contrast to the NRM. However, when compared with the PCA–FEM method, the proposed method can make controllable deformation by considering different local and global deformations. In addition, we can easily warp a high-resolution model with more than 10 K vertices with cost-effective computation thanks to two linear computations: CBD and Laplace–Beltrami equation. Furthermore, the mesh decimation algorithm, which reduces the number of mesh vertices to reach fewer cage handles, helps to implement this linear computation. Comparing the data enlargement in CCBD with methods like focused shape models proposed by the Chandra et al. shows that the focused shape approach has been proposed for the applications with a desired anatomical structure or region of clinical interest [11]. In contrast, the CCBD models complete organs, so the SSM should provide variations in the entire structure in addition to the maintaining local disparities. In such cases, enlarging the training datasets can solve the problem, although it may not be the only solution.

The created models through the CCBD have real appearances as shown in Fig. 6. In addition, the amount of changes made is displayed in color code. For example, the highest change, which is indicated by red, is related to the femoral head. However, in the two lower cases, most changes are related to the lower femur. The same is true for the liver. There are three reasons for this.

First, various handles are chosen as the main handle. Therefore, the points that are closest to the selected handle have the most amount of variation. This has been shown in Fig. 6 in red areas. Connecting different handles to each other, one of the other reasons, causes a local displacement of a handle to lead to a general shape deformation. Finally, selecting different stiffness for handles results in different degrees of deformation in each part of the mesh. These reasons make it possible to create different artificial instances by choosing different starting handles.

To reduce the data exclusion rate via human filtering, the parameters influence the generation of artificial data such as stiffness and handle movement, experimentally are bounded to make a reasonable result. So, most of the generated data are rational from an expert point of view, and only the extraordinary outliers are eliminated. The results prove that if the number of outliers compared to the all generated data be negligible, data elimination is not a vital step. By the way, this step is proposed to improve the generalization ability of the proposed algorithm.

In conclusion, using the CCBD gives more control over morphing the mesh, which makes it possible to produce real samples and increases computational speed. It also helps to enrich the SSMs ability, especially in predicting unseen instances and in the case of data shortage.

Conclusion

Although the SSMs are of great interest in many medical applications for image analysis [1, 2] such as segmentation [6, 12, 44, 45], registration [3, 4] and shape deformation [5], their access to sufficient data is the key point in their success rate. In this paper, we proposed a new approach using CBD and linear Laplace–Beltrami equation to address this problem. To the best of our knowledge, this is the first time that the CBD accompanying the Laplace–Beltrami equation has been used to construct SSM. By the proposed two-step deforming approach, once a handle is selected as an initial point of the deformation, the constraints affect the deformation and have an impact on both the local and global deformations.

Using the proposed CCBD in SSM data enrichment has two major advantages; first, by calculating the blending coefficients via the bounded bi-harmonic blending method, real appearance is preserved during the deformation [26, 27]. Therefore, obtained instances can be very close to the natural ones. Second, the limited number of handles, which resulted from the mesh decimation algorithm, compared with the number of base model vertices, makes the warping possible with cost-effective computation.

In the evaluating step, we compared our method with other well-known artificial data enlargement applications. The results of the generalization ability test show a promising promotion over other methods. In addition, the specificity of the CCBD shows a relative improvement for the liver and femur.

As the next step, we are going to apply our method in other parts of the body, such as the spine. The similarity of the spine vertebrae, despite the differences between them, can promise the application of our proposed method for the Enhanced SSM generation of the spine, particularly in partial observations and data limitation condition.

Similarly, the idea of using the handles around the 3D model of medical data can be utilized as a new paradigm in applications such as segmentation and registration.

Acknowledgements The authors gratefully acknowledge the support and generosity of Fanavaran Jarahyar Sharif Co. for providing Femur dataset that without which the present study could not have been completed. We are also immensely grateful to Seyed Mohammad Reza Noori for comments that significantly improved the manuscript.

Funding This work was supported by the medical school, Tehran University of Medical Science in Grant Number 28345 and also by the Iran National Science Foundation in Grant Number 92011635.

Compliance with ethical standards

Conflict of interest The authors declare that they have no conflict of interest.

Ethical approval This article does not contain any studies with human participants or animals performed by any of the authors.

References

1. Heimann T, Meinzer H-P (2009) Statistical shape models for 3D medical image segmentation: a review. Med Image Anal 13(4):543–563
2. Lüthi M (2010) A machine learning approach to statistical shape models with applications to medical image analysis. University_of_Basel, Basel
3. Gholipour A et al (2007) Brain functional localization: a survey of image registration techniques. IEEE Trans Med Imaging 26(4):427–451
4. Zitova B, Flusser J (2003) Image registration methods: a survey. Image Vis Comput 21(11):977–1000
5. Gain J, Bechmann D (2008) A survey of spatial deformation from a user-centered perspective. ACM Trans Graph (TOG) 27(4):107
6. Castro-Mateos I et al (2015) Statistical interspace models (SIMs): application to robust 3D spine segmentation. IEEE Trans Med Imaging 34(8):1663–1675
7. Yokota F et al (2009) Automated segmentation of the femur and pelvis from 3D CT data of diseased hip using hierarchical statistical shape model of joint structure. In international conference on medical image computing and computer-assisted intervention. Springer
8. Lamecker H, Lange T, Seebass M (2004) Segmentation of the liver using a 3D statistical shape model. Konrad-Zuse-Zentrum fur Informationstechnik, Berlin
9. Zhang X et al (2010) Automatic liver segmentation using a statistical shape model with optimal surface detection. IEEE Trans Biomed Eng 57(10):2622–2626
10. Martin S, Troccaz J, Daanen V (2010) Automated segmentation of the prostate in 3D MR images using a probabilistic atlas and a spatially constrained deformable model. Med Phys 37(4):1579–1590
11. Chandra SS et al (2014) Focused shape models for hip joint segmentation in 3D magnetic resonance images. Med Image Anal 18(3):567–578
12. Albà X et al (2014) Reusability of statistical shape models for the segmentation of severely abnormal hearts. In: international workshop on statistical atlases and computational models of the heart. Springer, New York
13. Lötjönen J et al (2005) Artificial enlargement of a training set for statistical shape models: application to cardiac images. In international workshop on functional imaging and modeling of the heart. Springer
14. Van Assen HC et al (2005) SPASM: segmentation of sparse and arbitrarily oriented cardiac MRI data using a 3D-ASM. In international workshop on functional imaging and modeling of the heart. Springer
15. Mitchell SC et al (2002) 3-D active appearance models: segmentation of cardiac MR and ultrasound images. IEEE Trans Med Imaging 21(9):1167–1178
16. Davatzikos C, Tao X, Shen D (2003) Hierarchical active shape models, using the wavelet transform. IEEE Trans Med Imaging 22(3):414–423
17. Chung F et al (2011) Comparison of statistical models performance in case of segmentation using a small amount of training datasets. Visual Comput 27(2):141–151
18. Ordas S, et al (2004) Grid-enabled automatic construction of a two-chamber cardiac PDM from a large database of dynamic 3D shapes. In IEEE International Symposium on Biomedical Imaging: Nano to Macro, 2004. IEEE
19. de Bruijne M et al (2003). Adapting active shape models for 3D segmentation of tubular structures in medical images. In biennial international conference on information processing in medical imaging. Springer
20. Hu N et al (2014) A method for generating large datasets of organ geometries for radiotherapy treatment planning studies. Radiol Oncol 48(4):408–415
21. Pereañez M (2017) Enlargement, subdivision and individualization of statistical shape models: application to 3D medical image segmentation
22. Pereañez M et al (2014) A framework for the merging of pre-existing and correspondenceless 3D statistical shape models. Med Image Anal 18(7):1044–1058
23. Ehrhardt J, Wilms M, Handels H (2016) Patch-based low-rank matrix completion for learning of shape and motion models from few training samples. In European conference on computer vision. Springer
24. Cootes TF, Taylor CJ (1995) Combining point distribution models with shape models based on finite element analysis. Image Vis Comput 13(5):403–409
25. Koikkalainen J et al (2008) Methods of artificial enlargement of the training set for statistical shape models. IEEE Trans Med Imaging 27(11):1643–1654
26. Jacobson A et al (2011) Bounded biharmonic weights for real-time deformation. ACM Trans Graph 30(4):1–8
27. Ju T, Schaefer S, Warren J (2005) Mean value coordinates for closed triangular meshes. In ACM transactions on graphics (TOG). ACM
28. Lipman Y et al (2007) GPU-assisted positive mean value coordinates for mesh deformations. In symposium on geometry processing
29. Joshi P et al (2007) Harmonic coordinates for character articulation. In: ACM transactions on graphics (TOG). ACM
30. Wang Y, Staib LH (2000) Physical model-based non-rigid registration incorporating statistical shape information. Med Image Anal 4(1):7–20
31. Cootes TF, Taylor CJ (1996) data driven refinement of active shape model search. In: BMVC
32. Zhang S, Zhan Y, Metaxas DN (2012) Deformable segmentation via sparse representation and dictionary learning. Med Image Anal 16(7):1385–1396
33. Fang Q, Boas DA (2009) Tetrahedral mesh generation from volumetric binary and grayscale images. In: IEEE International Symposium on Biomedical Imaging: From Nano to Macro, 2009. ISBI'09. IEEE
34. Hussain M, Okada Y, Niijima K (2004) *Efficient and feature-preserving triangular mesh decimation*. In *WSCG*
35. Meyer M et al (2002) Generalized barycentric coordinates on irregular polygons. J Graph Tools 7(1):13–22
36. Jacobson A et al (2011) Bounded biharmonic weights for real-time deformation. ACM Trans Graph 30(4):78:1–78:8
37. Floater MS (2003) Mean value coordinates. Comput Aided Geom Des 20(1):19–27
38. Lipman Y, Levin D, Cohen-Or D (2008) Green coordinates. ACM Trans Graphics (TOG) 27(3):78

39. Lipman Y et al (2004) Differential coordinates for interactive mesh editing. In: Proceedings shape modeling applications. IEEE
40. Meyer M et al (2003) Discrete differential-geometry operators for triangulated manifolds. Visualization and mathematics. Springer, New York, pp 35–57
41. Feldmar J et al (1997) Extension of the ICP algorithm to nonrigid intensity-based registration of 3D volumes. Comput Vis Image Underst 66(2):193–206
42. Jolliffe IT (2002) Principal component analysis and factor analysis. Princ Compon Anal 69:150–166
43. Davies RH (2002) Learning shape: optimal models for analysing natural variability. University of Manchester, Manchester
44. Pham DL, Xu C, Prince JL (2000) Current methods in medical image segmentation. Annu Rev Biomed Eng 2(1):315–337
45. Lenkiewicz P et al (2010) Techniques for medical image segmentation: review of the most popular approaches. Biomedical diagnostics and clinical technologies: applying high-performance cluster and grid computing. University of Beira Interior, Covilha, pp 1–33